Journal of Food Engineering 171 (2016) 57–66

Contents lists available at ScienceDirect

Journal of Food Engineering

journal homepage: www.elsevier.com/locate/jfoodeng

Rheological characterization of full-fat and low-fat glaze materials for foods

Bárbara E. Meza*, Juan Manuel Peralta, Susana E. Zorrilla

Instituto de Desarrollo Tecnológico para la Industria Química (INTEC), Universidad Nacional del Litoral – CONICET, Güemes 3450, S3000GLN Santa Fe, Argentina

ARTICLE INFO

Article history:
Received 27 July 2015
Received in revised form
29 September 2015
Accepted 8 October 2015
Available online 22 October 2015

Keywords:
Rheology
Glaze material
Food coating
Fat mimetic

ABSTRACT

The objective of this work was to perform the rheological characterization of full-fat and low-fat glaze materials used as film-forming fluids. Glaze materials were elaborated with icing sugar, skim milk powder, water, and different contents (0, 3, 6, and 9%) of vegetable fat (sunflower oil and soy lecithin) or microparticulated whey protein as fat mimetic. Rotational rheometry, creep tests, and dynamical rheometry were performed. Yield stress was obtained by direct and indirect methods. Steady shear viscosity was analyzed applying the Herschel–Bulkley model. Complex moduli were modeled with a power law equation and the application of Cox–Merz rule was considered. Images were obtained by optical microscopy. Average film thickness values were estimated using a mechanistic mathematical model for a dip-coating process during the draining stage. The results indicated that it may be possible to obtain low-fat glaze materials with rheological properties, microstructure, and film thickness-forming capacities similar to full-fat formulations.

1. Introduction

In the food industry, glazing (or icing) refers to the application of a coating glaze material onto the food surface to produce a homogeneous gloss film that enhances its shine and appearance. Besides improving the food aspect, this technique can also give a moisture-barrier protection to contribute in extending the shelf-life of bakery and confectionery products (Fog-Petersen and Skibsted, 1999; Jahromi et al., 2012; Lee et al., 2002).

Glaze materials used as film-forming fluids can be made with protein-based components (milk, egg, etc.) and fat-based components (shortening, cocoa butter, vegetable oil, etc.). However, the main ingredient of a glaze material is usually sugar (Nieto, 2009). As consequence, an improvement in the flavor and texture of the final food product is expected before glazing. For example, if a small amount of egg protein (powdered albumen or fresh egg white) is added into the sugar-base glaze formulation, the hardness of the layer over the food surface is increased before drying (Buckman and Viney, 2002). Before baking, glaze materials can interact chemically with the crust, delaying the dehydration and allowing increased product expansion of confectionery and bakery products (Chin et al., 2011). In addition, Maillard reactions and caramelization process can take place in the glaze film during baking. This phenomenon produces desirable changes in the color (turning dark and brown) and flavor of foods, due to the presence of egg proteins and sucrose (Fog-Petersen and Skibsted, 1999). Furthermore, the existence of a lipid phase in glaze materials (such as shortening) has produced lower crust firmness, creating bread with softer crust and harder crumb than control (Chin et al., 2011).

Fat-based components present in foods are associated with organoleptic and sensory acceptability by consumers. However, around the world there is an increased consumer demand for low-fat food products, due principally to a more awareness of health risks associated with high-fat diets (Poirier et al., 2006). For this reason, the development of high quality food products with reduced fat is a high priority for the food industry (Sandrou and Arvanitoyannis, 2000).

The reduction of fat in manufactured foods, for example dairy and meat products, was associated with technological problems such as a decrease in texture quality and a modification in their rheological properties (Yang et al., 2011; Galanakis et al., 2010). The use of fat replacers has been implemented as a strategy for quality improvement, because they can be incorporated into the low-fat food products in order to maintain the sensory consumer

* Corresponding author.
E-mail address: bmeza@intec.unl.edu.ar (B.E. Meza).

http://dx.doi.org/10.1016/j.jfoodeng.2015.10.012
0260-8774/

acceptability characteristics of their full-fat counterparts (O'Connor and O'Brien, 2011).

Fat mimetics (typically protein- or carbohydrate-based molecules) are a kind of fat replacer that can mimic some of the organoleptic and physical properties of conventional fat. Microparticulated whey proteins are an example of a protein-based fat mimetic used to give creamy and smooth texture to a great number of low-fat food products (Singer, 1996). Whey proteins can be considered as an attractive ingredient for the manufacture process of low-fat film-forming fluids. However, investigations related to this topic were not extensively found in literature (Gómez, 2008; Laneuville et al., 2005; Lee et al., 2002).

The knowledge of the rheological properties is significant for both food engineering process design and food quality control (Steffe, 1996). In coating technology, rheological properties are important because some physical phenomena that occur during this procedure, like draining (sagging or slumping) and leveling, are influenced by the rheological behavior of the film-forming fluid (Chan and Venkatraman, 2006). From the literature reviewed, the final film thickness was influenced by the viscosity and the magnitude of the yield stress of the film-forming fluid (milk chocolate, molten ice cream compound coatings, malt dextrin and malt suspensions) (Bhattacharya and Patel, 2007; Ghorbel et al., 2011; Karnjanolarn and McCarthy, 2006). Although several coating methods are used in food industry, dip coating is considered a simple and economical technique for many practical situations, like in ice-cream manufacturing or in chocolate enrobing process (Ghorbel et al., 2011; Wichchukit et al., 2005). During dip coating, the substrate is immersed into a reservoir containing the film-forming fluid for a period of time. After that, the withdrawing of the substrate from the bath and the fluid drainage by gravity complete the film formation (Grosso, 2011).

In recent years, there have been few studies about glazing application on food products, although glazing is a common practice in baking and confectionery industry (Buckman and Viney, 2002; Chin et al., 2011; Fog-Petersen and Skibsted, 1999; Jahromi et al., 2012). The rheological characterization of glaze materials, especially with different fat and fat mimetic contents, was not found in literature. This knowledge can be useful to control and predict the film thickness during an industrial food glazing process, reducing the amount of trial-and-error effort in obtaining a desirable homogenous gloss film (Meza et al., 2015). The objective of this work was to perform the rheological characterization of full-fat and low-fat glaze materials used as film-forming fluids in food coating processes. Average film thickness values were estimated using a mechanistic mathematical model for a dip-coating process of a plate during the draining stage previously published (Peralta et al., 2014a,b).

2. Materials and methods

2.1. Materials

Icing sugar (Borgato y Pirola S.R.L., Santa Fe, Argentina), sunflower oil (Molinos Río de la Plata S.A., Buenos Aires, Argentina), and soy lecithin (Laboratorios Yeruti S.R.L., Santa Fe, Argentina) were purchased in local markets. Skim milk powder (SanCor Coop. Unidas Ltda., Santa Fe, Argentina) was obtained from a local shop and the composition supplied by the manufacturer was: 50% carbohydrate, 36% protein, and 0% fat. Moisture content, determined by standard procedure (IDF, 1993), was 3.0 ± 0.1%. Microparticulated whey proteins (MWP) powder (Simplesse Dry100®, CPKelco US Inc., Atlanta, GA) was used as fat mimetic. The composition supplied by the manufacturer was: 52.9% protein, 4.8% fat, and 2.9% moisture.

2.2. Elaboration of glaze materials

Glaze materials used as film-forming fluids in food coating processes were elaborated following the recipe shown in Table 1. All formulations were proposed taking into account the local legislation (CAA, 2010) and were elaborated according to the methodology used by Chin et al. (2011) with modifications.

In order to elaborate samples with different fat contents, the appropriate amount of icing sugar and skim milk was placed in a bowl and dissolved in distilled water with a manual whisk during 3 min to obtain a suspension. Soy lecithin, used as fat emulsifier, was dissolved in the vegetable oil. After that, the lipid phase was incorporated into the suspension by hand using a manual whisk during 3 min in order to obtain glaze materials with 3, 6, and 9% of fat content. The inclusion of lecithin, a lipid-based ingredient, was considered as part of the fat fraction in every formulation (Table 1). On the other hand, to elaborate samples with different contents of fat mimetic, the appropriate amount of icing sugar, skim milk, and MWP was placed in a bowl and dissolved in distilled water with a manual whisk during 3 min to obtain suspensions with 3, 6, and 9% of fat mimetic content.

Each glaze material was degassed during 15 min at vacuum conditions (0.3 atm) to remove visible bubbles. Subsequently, samples were placed in hermetic plastic containers with a plastic film over the surface to avoid crust formation and stored at 5 °C during 24 h for further analysis. The film-forming capacity of glaze materials was confirmed by dip-coating technique (Fig. 1). All formulations were prepared by triplicate, being stable without phase separation within the experimental time.

2.3. Rheological characterization

2.3.1. Rheological measurements

Rheological measurements at 20.0 ± 0.5 °C were done by duplicate using a stress controlled rheometer (RheoStress 80, Haake Inc. Instruments, Germany) with a cone and plate sensor geometry (cone angle = 2°; diameter = 35 mm). Before measurements, each sample rested during 180 s allowing relaxation. A thin film of silicone oil (100 cP) was applied to the exposed sample edges to prevent water vaporization during measurements.

Rotational rheometry was performed in the shear rate range of 0.5–100 s^{-1}. Values of steady shear viscosity ($\eta(\dot{\gamma})$) as function of shear rate ($\dot{\gamma}$) were determined.

Creep tests were performed applying a range of shear stress from 1 to 300 Pa during 5 min. Values of strain (γ) as function of shear stress (τ) were obtained.

Dynamical rheometry was carried out performing frequency sweeps (1–10 rad s^{-1}) in the linear viscoelastic region (LVR) at constant stress amplitude (5 Pa). Prior to each frequency sweep, a stress sweep (1–300 Pa) was done at the maximum frequency

Table 1
Recipe used to manufacture glaze materials with different fat and fat mimetic contents.

Code	Ingredients [%] (w/w)				
	Icing sugar	Skim milk	Fat[a]	MWP[b]	Water
Control	50	20	0	0	30
Fat 3%	50	20	3	0	27
Fat 6%	50	20	6	0	24
Fat 9%	50	20	9	0	21
MWP 3%	50	20	0	3	27
MWP 6%	50	20	0	6	24
MWP 9%	50	20	0	9	21

[a] Fat = sunflower oil (2, 5, and 8%) and 1% of soy lecithin.
[b] MWP = microparticulated whey protein (fat mimetic).

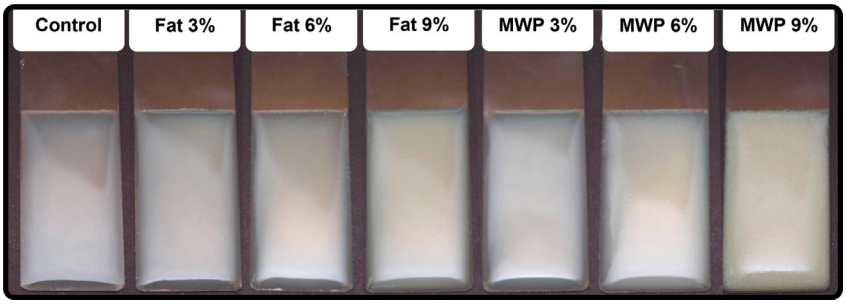

Fig. 1. Films obtained by dip-coating technique using glaze materials manufactured according to the proposed recipe (Table 1).

(10 rad s^{-1}) in order to determine the LVR. Values of storage ($G'(\omega)$), loss ($G''(\omega)$), and complex ($|G^*(\omega)|$) moduli were determined.

2.3.2. Yield stress

The presence of yield stress was analyzed by both direct and indirect methods, taking into account the practical definition of yield stress as any critical stress below which no flow can be observed under the condition of experimentation (Nguyen and Boger, 1992).

Static yield stress ($\tau_{0,s}$) was obtained by a direct method, using the experimental data from creep tests. Log–log plots of strain versus shear stress were analyzed and the intersection between the two linear segments (obtained by linear regression) was considered as an estimated value of the static yield stress (Fig. 2*a*) (Bhattacharya, 1999; Steffe, 1996).

Dynamic yield stress ($\tau_{0,d}$) was obtained by an indirect method, fitting the experimental data of shear rate versus steady shear stress to a polynomial equation and extrapolating the data to zero shear rate (Fig. 2*b*) (Nguyen and Boger, 1992; Moelants et al., 2013; Peressini et al., 2003).

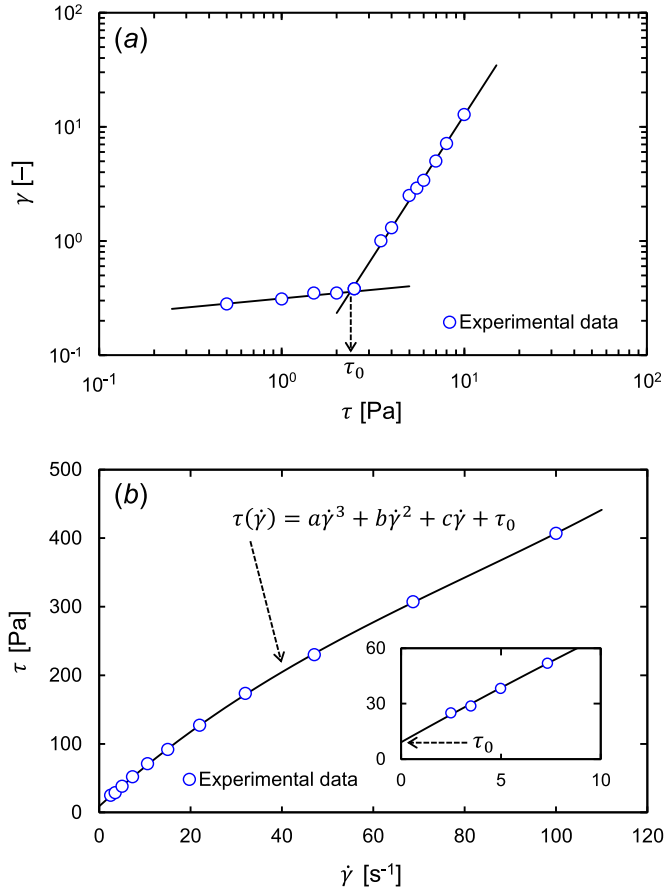

Fig. 2. Examples of the methodology used to obtain the yield stress. (*a*) Static yield stress estimated by creep test and (*b*) dynamic yield stress obtained by polynomial regression and extrapolation to shear rate equal to zero. Symbols are experimental values and lines represent the regression.

2.3.3. Modeling the rheological behavior

Steady shear viscosity as function of shear rate was analyzed using the Herschel–Bulkley model (Steffe, 1996):

$$\eta(\dot{\gamma}) = \tau_0 \dot{\gamma}^{-1} + K\dot{\gamma}^{n-1} \tag{1}$$

where τ_0 is the yield stress, K is the consistency index, and n is the behavior index. According to Rao (2007), if τ_0 of the sample is known from an independent experiment, K and n can be determined by regression. In this study, in order to reduce conveniently the number of parameters for model regression, τ_0 values were considered as equal to $\tau_{0,d}$ values obtained using the methodology described in Section 2.3.2.

Storage and loss moduli as function of frequency were analyzed using the power law model (Steffe, 1996):

$$G'(\omega) = a\omega^b \tag{2}$$

$$G''(\omega) = c\omega^d \tag{3}$$

where ω is the angular frequency and parameters a, b, c, and d are constants that depend on the material nature. For the particular case where ω is equal to 1 rad s^{-1}, a and c are equal to the storage and loss moduli at that frequency, respectively.

2.3.4. Cox–Merz rule

The Cox–Merz rule expresses that the complex viscosity ($|\eta^*(\omega)|$) is near equal to the steady shear viscosity when $\omega = \dot{\gamma}$ for arbitrary frequencies or shear rates (Bird et al., 1987; Cox and Merz, 1958):

$$\left|\eta*(\omega)\right|_{\omega=\dot{\gamma}} = \eta\prime(\omega)\left[1+\left(\frac{\eta''(\omega)}{\eta\prime(\omega)}\right)^2\right]^{\frac{1}{2}}\Big|_{\omega=\dot{\gamma}} \approx \eta(\dot{\gamma}) \tag{4}$$

where $\eta'(\omega)$ and $\eta''(\omega)$ are the loss and storage viscosities, respectively. At low shear rates, where the stress and strain relation is linear, the Cox–Merz rule holds identically according to the following expression:

$$\lim_{\omega\to 0} |\eta^*(\omega)|_{\omega=\dot{\gamma}} = \eta'(\omega)\Big|_{\omega=\dot{\gamma}} = \eta(\dot{\gamma}) \tag{5}$$

Taking into account that $|\eta^*(\omega)|\omega = |G^*(\omega)|$ and $\eta(\dot{\gamma})\dot{\gamma} = \tau(\dot{\gamma})$,

where $\tau(\dot{\gamma})$ is the steady shear stress, the validity of the Cox–Merz rule is maintained by multiplying both factors by ω and $\dot{\gamma}$, respectively (Winter, 2009):

$$|\eta^*(\omega)|_{\omega=\dot{\gamma}}\omega \approx \eta(\dot{\gamma})\dot{\gamma} \tag{6}$$

$$|G^*(\omega)|_{\omega=\dot{\gamma}} \approx \tau(\dot{\gamma}) \tag{7}$$

The application of the Cox–Merz rule by representing experimental data using Eq. (7) should give identical conclusions than those obtained with the original expression. However, although the selection of the methodology (Eq. (4) or (7)) is purely by convenience, in some practical cases the alternative representation of the Cox–Merz rule proposed by Winter (2009) allowed visualizing differences between material states in a clearer way (Snijkers and Vlassopoulos, 2014; Winter, 2009).

2.4. Optical microscopy

Images of each glaze formulation and ingredients (icing sugar, skim milk, fat, and MWP) were captured using a transmitted polarized light microscope (Olympus BH–2, Tokyo, Japan). Samples were prepared according to the recipe described in Table 1 and, in order to obtain representative images of each ingredient separately, suspensions of icing sugar (50%), skim milk (20%), and MWP (9%) were elaborated. In addition, an emulsion with 9% of fat (8% of sunflower oil and 1% of soy lecithin) was used. An aliquot of each sample was placed between two glass slides separated by 0.2 mm. After that, slides were observed with the microscope at 20× magnification and 100% intensity, obtaining five photomicrographs for each sample.

2.5. Density

Experimental density of each glaze formulation at 20 °C was determined gravimetrically by quintuplicate weighing a recipient with known volume (1.83 cm^3) and containing an aliquot of sample (Meza et al., 2015).

2.6. Average film thickness

Theoretical average film thickness values were estimated using the mechanistic mathematical model proposed by Peralta et al. (2014a, b) for a dip-coating process of a vertical plate. A particular solution of this model for the draining stage considering that the rheological behavior of the film-forming fluid is described by the Herschel–Bulkley equation (Eq. (1)) can be expressed as follows:

$$\frac{\langle h\rangle}{h} = \frac{(nS_{\tau_0})^2 + nS_{\tau_0} + (n+1)^2}{(2n+1)(n+1)} \tag{8}$$

$$\frac{\rho g_x h}{K} - \frac{\tau_0}{K} - \left(\frac{x}{ht}\right)^n = 0 \tag{9}$$

where $\langle h\rangle$ is the theoretical average film thickness, h is the film thickness at the x position of the plate, g_x is the gravity acceleration, S_{τ_0} is the ratio of the yield stress to the maximum stress ($\tau_0/(\rho g_x h)$), ρ is the density, and t is the time.

2.7. Statistical analysis

Values of $\tau_{0,s}$ were obtained using linear regression (Section 2.3.2). Values of $\tau_{0,d}$ were calculated by linear regression of shear rate versus steady shear stress data using a third order polynomial and the subsequent extrapolation of shear stress to shear rate equal to zero. Parameters K and n of Eq. (1) were obtained by nonlinear regression, while parameters of Eqs. (2) and (3) were estimated using linear regression. Analysis of variance was used and, when the effect of the factors was significant ($P < 0.05$), the Tukey's honestly significant difference multiple ranks test was applied (confidence level of 95%). In addition, root mean square errors (*RMSE*) were calculated:

$$RMSE = \sqrt{\frac{1}{N}\sum_{i=1}^{p}\left(x_{i,\mathrm{exp}} - x_{i,\mathrm{theor}}\right)^2} \tag{10}$$

where $x_{i,\mathrm{exp}}$ is the i-th experimental value, $x_{i,\mathrm{theor}}$ is i-th theoretical value, and N is the total number of samples. All statistical analysis was performed using Minitab 13.20 (Minitab Inc., State College, PA).

3. Results and discussion

3.1. Characterization of the flow behavior

Values of steady shear viscosity as function of shear rate for glaze materials with different fat and fat mimetic contents are shown in Fig. 3. All formulations presented a shear-thinning behavior, where $\eta(\dot{\gamma})$ decreases as $\dot{\gamma}$ increases. However, this behavior is more evident in samples with fat and MWP contents higher than 3%. According to Rao (2007), a shear-thinning behavior may occur due to the breakdown of structural units in a food material by hydrodynamic forces generated during shear.

Values of static and dynamic yield stress are shown in Table 2. Static yield stress was observed only in glaze materials with the higher fat and MWP contents (Fat 9% > MWP 9% > MWP 6%). In these formulations, a clear slope change of strain was observed under the condition of experimentation (Fig. 2*a*). The other formulations did not show that pattern (data not shown). It is expected that dilute solutions and suspensions flow under very small stress. Therefore, it is possible that the static yield stress for those samples was too low to be detected under the experimentation conditions used in the present work.

Values of dynamic yield stress increase as the fat and MWP increase in glaze materials with fat and MWP contents higher than 3% (Table 2). No significant differences were obtained between $\tau_{0,d}$ values of Fat 9% and MWP 6% samples. Yield stress is an important rheological variable accepted for its practical usefulness in engineering design and processes operation where handling and

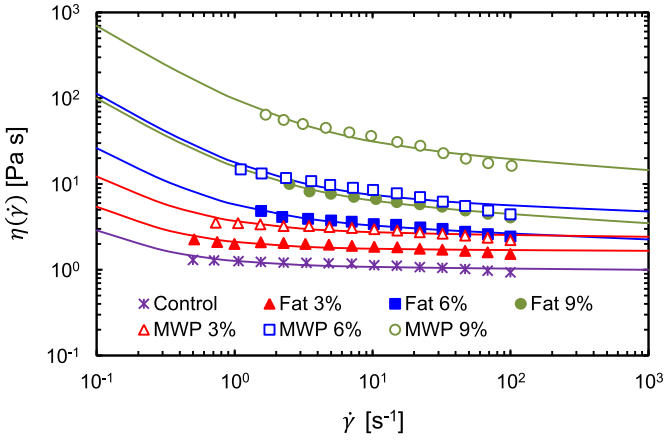

Fig. 3. Steady shear viscosity as function of shear rate obtained at 20 °C for glaze materials with different fat and fat mimetic contents. Symbols are experimental values and lines represent the Herschel–Bulkley model.

Table 2
Static yield stress ($\tau_{0,s}$), dynamic yield stress ($\tau_{0,d}$), and Herschel–Bulkley rheological parameters (K and n) obtained at 20 °C for glaze materials with different fat and fat mimetic contents.

Code	$\tau_{0,s}$[Pa]$^{+,*}$	$\tau_{0,d}$[Pa]$^{+,**}$	K [Pa s]$^{+}$	n [-]$^{+}$	*RMSE* [Pa s]
Control	–	0.21 ± 0.05[a]	1.09 ± 0.01[a]	0.98 ± 0.00[a]	0.07
Fat 3%	–	0.31 ± 0.07[a]	1.75 ± 0.00[b]	0.99 ± 0.00[a]	0.11
Fat 6%	–	2.28 ± 0.11[b]	3.38 ± 0.28[d]	0.94 ± 0.01[a]	0.15
Fat 9%	4.50 ± 0.00[c]	10.45 ± 1.92[c]	6.63 ± 0.44[e]	0.90 ± 0.00[b]	0.29
MWP 3%	–	0.83 ± 0.14[a]	2.80 ± 0.03[c]	0.98 ± 0.01[a]	0.21
MWP 6%	2.50 ± 0.00[a]	10.92 ± 0.69[c]	7.37 ± 0.13[e]	0.95 ± 0.02[a]	1.17
MWP 9%	3.00 ± 0.00[b]	69.71 ± 6.00[d]	29.85 ± 3.72[f]	0.90 ± 0.03[b]	4.00

$^{+}$ Mean values and standard deviations of two replicates.
* Estimated by creep tests.
** Estimated by extrapolation.
$^{a-f}$ Means within a column with different letters are significantly different (P<0.05).

transport of suspensions are involved (Nguyen and Boger, 1992; Rao, 2007). For example, the minimum pump pressure required to start a slurry pipeline, the leveling and holding ability of a film-forming fluid, and the entrapment of air in thick pastes are typical problems where knowledge of the yield stress is essential (Nguyen and Boger, 1992). Yield stress was related to the strength of the coherent network structure of a material, which depends on the particle–particle interactions that are affected by particle concentration, shape, and polydispersity (Bhattacharya, 1999; Yoo and Rao, 1995).

Values of consistency and behavior indexes are shown in Table 2. Values of K increase as the fat and MWP contents increase in all glaze materials. No significant differences were obtained between K values of Fat 9% and MWP 6% samples.

Values of n were in the range of 0.90–0.98, but only significant differences were obtained between n values for glaze materials with 9% of fat and MWP (Table 2). This observation indicates that the shear-thinning behavior increases in formulations with the highest contents of fat and MWP, being coincident with data plotted in Fig. 3. In addition, flow behavior indexes of glaze materials tend to be closer to Newtonian flow ($n \approx 1$) in samples with fat and MWP contents lower than 9% and also in control samples.

According to the obtained results, the Herschel–Bulkley model could be used to describe the rheological behavior of glaze materials with different fat and fat mimetic contents, obtaining acceptable *RMSE* values in the range of 0.07–4.00 Pa s (Table 2 and Fig. 3). In addition, taking into account the results obtained for the rheological parameters $\tau_{0,d}$, K, and n, it may be possible to obtain low-fat glaze materials with flow properties similar to a full-fat product manufactured with vegetable fat.

3.2. Characterization of the viscoelastic behavior

Stress sweeps of glaze materials are shown in Fig. 4. According to the experimental data, complex modulus of each formulation was constant, indicating that the LVR is extended all over the tested shear stress range (Steffe, 1996).

Changes in storage and loss moduli as function of frequency of glaze materials with different fat and MWP contents are shown in Fig. 5. All formulations presented a viscous-like behavior, where loss modulus was higher than storage modulus in the complete range of studied frequencies.

Values of rheological parameters for power law model are shown in Table 3. In all formulations, with the exception of MWP 9%, the magnitudes of b (slope of G') and d (slope of G'') were approximately equal to 2 and 1, respectively. These results correspond to the viscoelastic behavior of a dilute system (Ferry, 1970). The magnitudes of b and d in MWP 9% sample were lower than values obtained for other formulations, probably due to a more concentrated state, being the behavior of MWP 9% similar to a semi-diluted system.

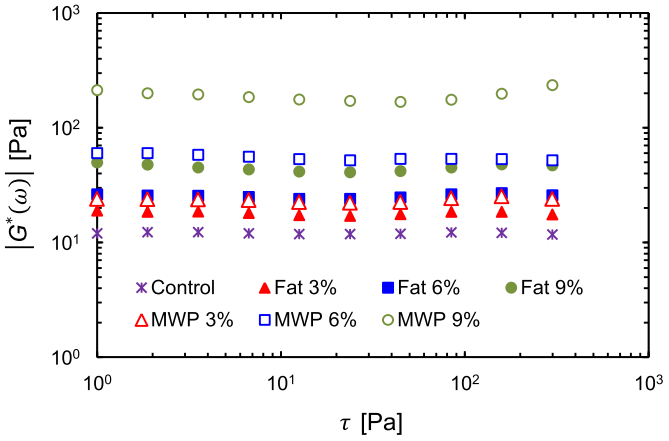

Fig. 4. Stress sweeps obtained at 20 °C and the maximum frequency (10 rad s^{-1}) for glaze materials with different fat and fat mimetic contents. Symbols are experimental values.

Values of c (G'' at 1 rad s^{-1}) increase as the fat and MWP contents increase in all glaze materials, being c the most representative viscoelastic parameter for the set of samples. No significant differences were obtained between c values of Fat 6% and MWP 3% samples and between c values of Fat 9% and MWP 6% samples. Taking into account that in these formulations the statistical analysis of the rest of power law parameters (a, b, and d) did not provide significant differences, the results obtained in this work indicate that this two set of samples (Fat 6% – MWP 3% and Fat 9% – MWP 6%) have similar viscoelastic behavior. In addition, the power law model may be used to describe the viscoelastic behavior of the studied glaze materials because acceptable *RMSE* values (0.05–1.54 Pa) were obtained (Table 3 and Fig. 5).

3.3. Cox–Merz rule

The application of the Cox–Merz rule to the experimental rheological data of glaze materials is shown in Fig. 6. The Cox–Merz rule was followed by control samples and formulations with the lowest contents of fat and MWP (Fat 3% and MWP 3%). In these cases, the flow and dynamic rheological data shown overlap and $|G^*(\omega)|_{\omega=\dot{\gamma}} \approx \tau(\dot{\gamma})$. However, the other formulations deviated from the Cox–Merz rule, showing $|G^*(\omega)|_{\omega=\dot{\gamma}} < \tau(\dot{\gamma})$.

The Cox–Merz rule has been applied to many polymer, colloidal, and food systems with varying degrees of success (Al-Hadithi et al., 1992; Yu and Gunasekaran, 2001). The essence of the Cox–Merz

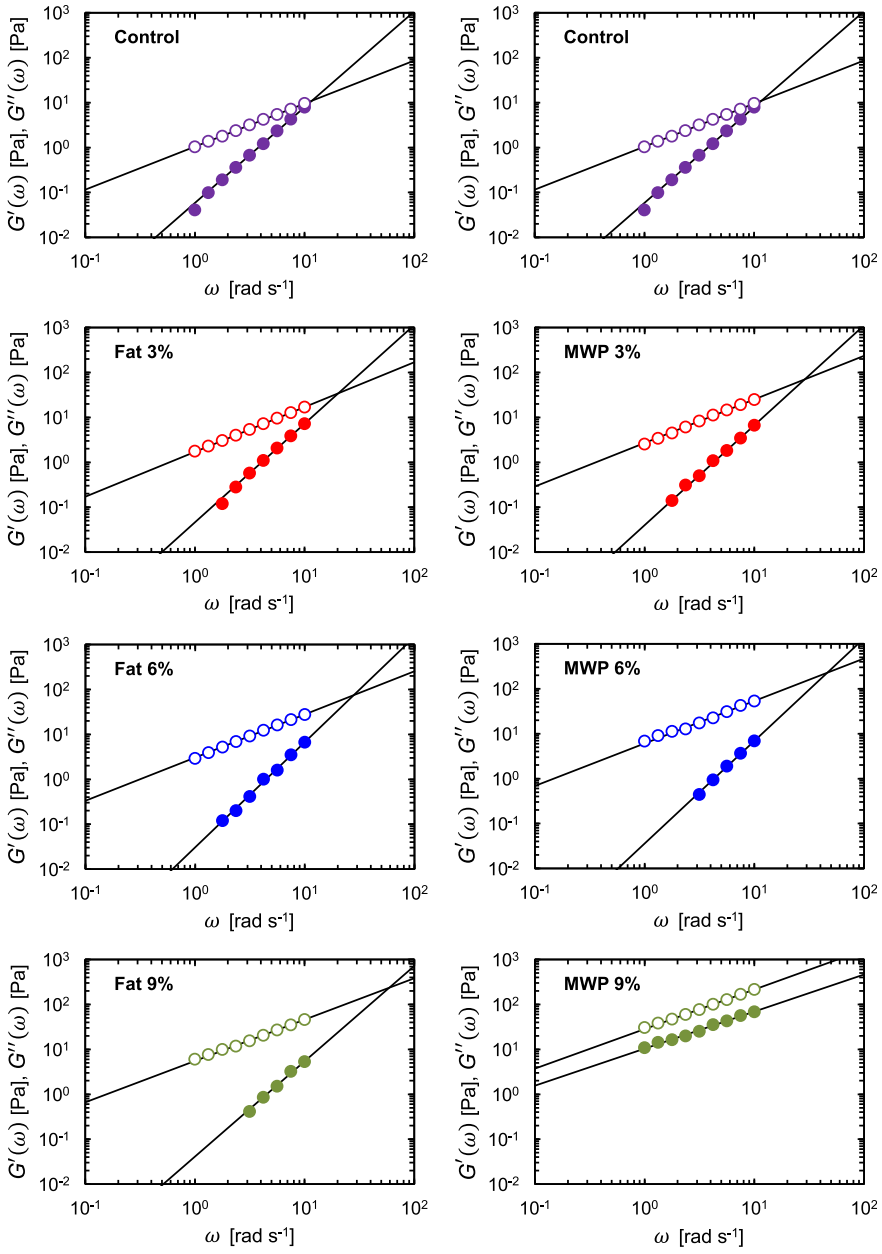

Fig. 5. Storage and loss moduli as function of frequency at 20 °C for glaze materials with different fat and fat mimetic contents manufactured according to the proposed recipe (Table 1). Symbols are experimental values and lines represent the power law model. (●) G'; (○) G''.

rule is the relationship between the linear (oscillatory) and nonlinear (steady state) viscosities (or their equivalent expressions) of a particular material. However, the practical application of the Cox–Merz rule lies in predicting steady shear rheological properties from linear oscillatory shear measurements. This valuable contribution, especially for industry, is based on oscillatory tests are

Table 3
Power law rheological parameters obtained at 20 °C for glaze materials with different fat and fat mimetic contents.

Code	a [Pa s^b]$^+$	b [-]$^+$	c [Pa s^d]$^+$	d [-]$^+$	*RMSE* [Pa]
Control	0.06 ± 0.00^a	2.11 ± 0.04^b	1.00 ± 0.07^a	1.00 ± 0.06^b	0.05
Fat 3%	0.04 ± 0.01^a	2.27 ± 0.10^b	1.76 ± 0.08^b	0.99 ± 0.01^b	0.07
Fat 6%	0.05 ± 0.02^a	2.18 ± 0.24^b	3.07 ± 0.04^c	0.97 ± 0.01^b	0.09
Fat 9%	0.03 ± 0.01^a	2.21 ± 0.12^b	5.18 ± 0.47^d	0.95 ± 0.04^b	0.31
MWP 3%	0.04 ± 0.00^a	2.25 ± 0.03^b	2.58 ± 0.17^c	0.99 ± 0.03^b	0.12
MWP 6%	0.04 ± 0.00^a	2.27 ± 0.02^b	6.08 ± 0.01^d	0.95 ± 0.00^b	0.66
MWP 9%	10.00 ± 0.54^b	0.80 ± 0.04^a	27.98 ± 0.47^e	0.88 ± 0.00^a	1.54

$^+$ Mean values and standard deviations of two replicates.
$^{a–d}$ Means within a column with different letters are significantly different ($P<0.05$).

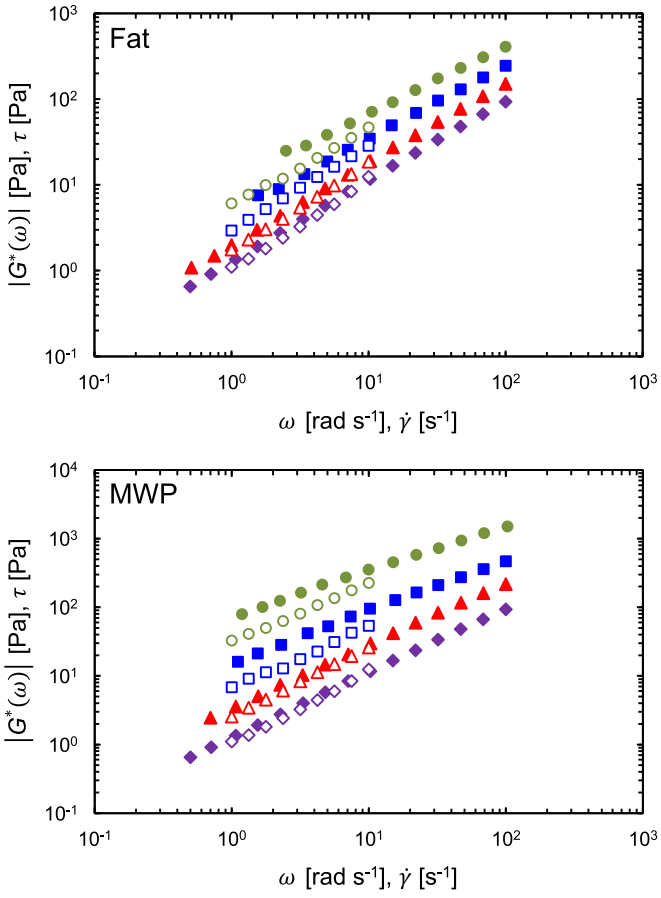

Fig. 6. Cox–Merz rule plots for glaze materials with different fat and fat mimetic contents. Symbols are experimental values. Open symbols:$|G^*(\omega)|$ and full symbols: $\tau(\dot{\gamma})$. ◊ ♦ Control, △ ▲ 3%, □ ■ 6%, ○ ● 9%.

relatively easy to perform on small sample quantities, while shear measurements are more difficult and are prone to instabilities and slippage (Snijkers and Vlassopoulos, 2014; Yu and Gunasekaran, 2001).

Although this rule has an empirical-based nature, a theoretical identical equality can be achieved in a limit case, where a linear behavior of the flow curve is expected (Eq. (5)). The physical fundamentals that explain why Cox–Merz rule applies in the nonlinear portion of the flow curve are still not clear (Mead, 2011; Snijkers and Vlassopoulos, 2014). On the other hand, in the particular case of food materials, the fail in the overlap of rheological properties during Cox–Merz rule application was attributed to possible structure presence and/or structure modifications within the material during assay. In this case, the most common departure from the Cox–Merz rule is observed when the linear rheological property is higher than the nonlinear one (for example, $|\eta^*(\omega)|_{\omega=\dot{\gamma}} > \eta(\dot{\gamma})$). This behavior was attributed to structure decay due to the effect of shear strain applied to the food system (Yu and Gunasekaran, 2001). The opposite behavior (for example, $|\eta^*(\omega)|_{\omega=\dot{\gamma}} < \eta(\dot{\gamma})$) is less common, but was also observed in several polysaccharides systems.

Xu et al. (2006) observed the last described behavior in Aeromonas gum (an exopolysaccharide) in aqueous solution. It was attributed to the heterogeneous nature of polysaccharide dispersions, that undergo aggregation, and to the highly branched structure of the polysaccharides. Since the Aeromonas gum easily forms aggregates in aqueous solution, the deviation from Cox–Merz rule was attributable to the formation of aggregates. In addition, with an increase in concentration $|\eta^*(\omega)|_{\omega=\dot{\gamma}} < \eta(\dot{\gamma})$ occurs at lower shear rate or frequency, suggesting that the formation of aggregates at high concentration is easier than at low concentration. Chamberlain and Rao (1999) observed similar behavior in waxy maize starch suspensions. It was also attributed to the heterogeneous nature of starch dispersions (that undergo aggregation) and to the highly branched structure of the starch. In addition, Lopes da Silva et al. (1993) reported similar observations in high-methoxyl pectin systems. Authors indicated that these systems are not true solutions, being two-phase systems with pectin micro-aggregates dispersed in the solvent.

The results obtained in this work indicate that in glaze materials with the highest contents of fat and MWP (Fat 9%, MWP 6%, and MWP 9%) the Cox–Merz rule failed. Lower complex modulus values rather than steady shear stress values were obtained in all the studied range of angular frequencies and shear rates. This behavior may be explained due to the heterogeneity of samples consisted of several phases, such as polysaccharide crystals, proteins, fat, and MWP, as will be discussed in the following section.

3.4. Optical microscopy

Photomicrographs of each ingredient and formulations (Table 1) are shown in Fig. 7. In the image corresponding to icing sugar, a clear visual field with few small crystals of sucrose (with rounded corners) can be observed. This result is expected because icing sugar is characterized to have fine crystals with low particle size distribution that confer high solubility capacity. Sucrose granulometry is an important property because coarse granulated sugar will yield a grainy and sandy texture, while fine crystals are preferable for a smooth and creamy consistency (Gómez, 2008).

The optical micrograph corresponding to skim milk shows high quantity of lactose crystals. These crystals are expected to be principally α-lactose due to their characteristic triangular or tomahawk shaped morphology (Garnier et al., 2002; Raghavan et al., 2000). According to the literature, metastable amorphous-stated lactose is formed during rapid spray drying of freshly milk powder. Amorphous lactose is very hygroscopic and can be quickly dissolved with the addition of water (Walstra et al., 2006). For this reason, if the dried milk powder is exposed to a water uptake storage conditions (high relative humidity and/or increased temperatures) the metastable amorphous lactose will precede through a transition to a stable crystalline state of α-lactose hydrate. These crystals are very hard, slightly hygroscopic, often large, and dissolve slowly (Jouppila et al., 1997; Lai and Schmidt, 1990; Walstra et al., 2006).

In fat image, vegetable oil drops stabilized by a soy lecithin layer are observed, while in MWP photo a high density of MWP with certain grade of interaction among microparticles can be observed. This image is similar to the results obtained by Renard et al. (2002), who reported an optical micrograph of a MWP suspension at high concentration (16%) after heat treatment. Authors described the optical micrograph with a particle gel-type structure with large flocs of MWP randomly connected after heating. However, Singer (1996) showed a light micrograph of a MWP suspension at low concentration (1.5%) where the individual or unconnected nature of microparticles was observed. Microparticulated whey proteins are a heterogeneous population of native soluble proteins and colloidal species that can be defined as soluble and insoluble aggregated proteins (Sanchez and Paquin, 1997; Sanchez et al., 1999). These microparticles are considered as highly structured protein-based complexes made from whey protein concentrates by a combination of several treatments such as acidification, heating, shearing, and/or high-pressure homogenization (Sanchez and Paquin, 1997; Singer et al., 1988; Spiegel, 1999). Despite the technology of

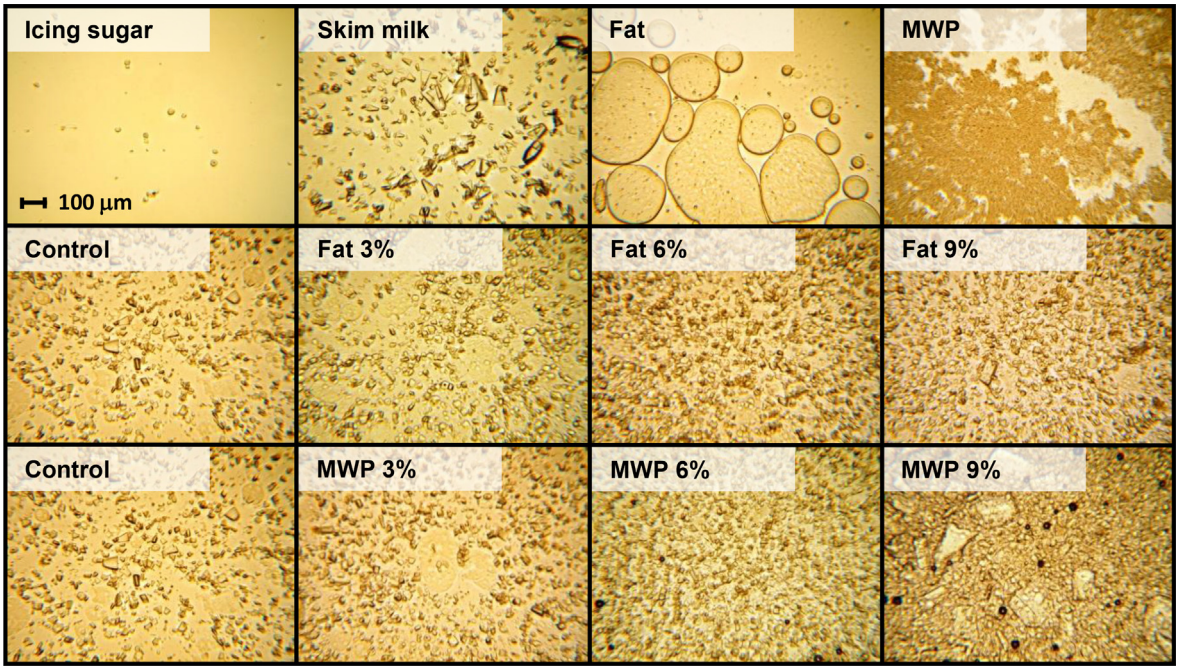

Fig. 7. Photomicrographs of glaze materials manufactured according to the proposed recipe (Table 1) and ingredients (icing sugar, skim milk, fat, and MWP).

manufacture used to obtain MWP, they have good water solubility that was attributed to an optimal unfolding of protein molecules and the stabilization of the protein aggregates by lactose via non-specific preferential hydration (Lieske and Konrad, 1994). For this reason, the results obtained in this work can be explained possibly due to the high concentration of the MWP suspension that could favor the interactions among microparticles in the condition of microscopy observation.

Optical micrograph corresponding to control sample is shown in Fig. 7. Image evidences high quantity of small crystals without cohesion. They are probably consisting in sucrose and lactose crystals, because principally to formulation composition (50% icing sugar and 20% skim milk) and their morphological shape. Sucrose crystals can present a rather complex structure of surfaces, being a prismatic three-dimensional shape representation one of the possible forms of such crystals (Faria et al., 2003). Buckman and Viney (2002) reported that the microstructure of a glaze material (glaze elaborated with 10 g icing sugar and 3 mL water) is dominated by large prismatic crystals in a light microscopy image. The authors indicated that little evidence of cohesion between crystals was observed.

Photomicrographs of glaze materials with different fat contents are shown in Fig. 7. The presence of small crystals increases as the fat content increases from control samples with 0% to samples with 9% of fat content. In addition, a continuous lipid phase can be observed in all images. The consequence of an increment in fat content is the reduction in the water content and the subsequent lactose and sucrose concentration. The crystallization of both lactose and sucrose in saturated solutions was early observed by Nickerson and Patel (1972). Although the crystallization rate was influenced by changes in sucrose-lactose balance, the general results suggested that lactose was less soluble than sucrose and a reduction in lactose solubility in presence of high concentrations of sucrose is expected. In addition, authors indicated that the mixing of lactose and sucrose modified the crystal-forming habits and shapes of both carbohydrates in solution.

Photomicrographs of glaze materials with different MWP contents are shown in Fig. 7. The presence of crystals increases as the MWP content increases from control samples with 0% to samples with 9% of MWP content. However, the boundaries between crystals are difficult to distinguish and they seem not to represent abrupt discontinuities in glaze materials microstructure. A continuous phase with the presence of MWP particles can be observed in all images. According to Janhøj and Ipsen (2006), the remaining native protein present in MWP can react with other proteins, and thus be integrated into the protein network. Some small lipid particles/vesicles can also be observed in the micrographs. According to Sanchez and Paquin (1997), residual lipids that are present in microparticulated whey protein concentrates can be organized in pseudo-membranes, that are visible through microscopy techniques, and may have an effect on the surface properties of MWP.

As it is expected, the consequence of an increase in MWP content is the reduction of the water content and the subsequent lactose and sucrose concentration. Formulation with the highest content of MWP (MWP 9%) had a particular appearance, where small bubbles (dark spheres) and high size crystals with an irregular shape can be observed. Although degasification process was taken place during glaze material elaboration in order to remove visible bubbles (Section 2.2), the high viscosity of this particular formulation could hinder the complete bubble removal with the consequent retention of small bubbles into the glaze matrix material. Buckman and Viney (2002) observed the presence of smooth spherical voids that were created by trapped air bubbles in royal icing. On the other hand, sucrose crystallization is a complex phenomenon that occurs through mechanisms of nucleation, growth, and agglomeration of crystals (Faria et al., 2003; Mathlouthi and Genotelle, 1998). Crystallization is affected by operating conditions, being the presence of impurities the most relevant situation. In particular, the agglomeration phenomenon has significant effect on the crystal size distribution and on the crystal aspect, generating quickly large and over size crystals (Faria et al., 2003).

It is interesting to notice that microphotos obtained for samples with 6% of fat and 3% of MWP and samples with 9% of fat and 6% of

Table 4
Values of experimental density (ρ) and estimated theoretical average film thickness ($\langle h \rangle$) obtained with Eqs. (8) and (9) for glaze materials with different fat and fat mimetic contents.

Code	ρ [kg m^{-3}][a]	$\langle h \rangle$ [mm]
Control	1352 ± 13	0.23
Fat 3%	1355 ± 20	0.30
Fat 6%	1368 ± 17	0.48
Fat 9%	1356 ± 25	1.08
MWP 3%	1406 ± 9	0.38
MWP 6%	1404 ± 12	1.09
MWP 9%	1410 ± 14	5.36

[a] Mean values and standard deviations of five replicates.

MWP had similar characteristics.

3.5. Theoretical average film thickness

Values of theoretical average film thickness of the analyzed glaze materials are shown in Table 4. These values were obtained with Eqs. (8) and (9) using experimental density values (Table 4) and rheological parameters ($\tau_{0,d}$, K, and n) of the Herschel–Bulkley model (Table 2). The length of the vertical plate and the draining time were 40 mm and 30 s, respectively, following the methodology proposed previously (Meza et al., 2015). The mechanistic mathematical model applied in this work was validated with experimental data from many sources (Meza et al., 2015; Peralta et al., 2014b). For this reason, it was considered that theoretical average film thickness values predicted in the present work can be used as a first step to analyze the effect of fat and MWP contents on the film thickness of glaze materials during a hypothetical food coating process.

The ranges of average film thickness that can be obtained with glaze materials elaborated with fat and MWP are 0.30–1.08 mm and 0.38–5.36 mm, respectively. As the fat and MWP contents increase in the formulations, average film thickness values increase. In the particular case of formulations Fat 9% and MWP 6%, the predicted average film thickness values were similar ($\approx$1.1 mm), showing the same pattern of response than the rheological parameters (Table 2).

4. Conclusions

The rheological characterization of full-fat and low-fat glaze materials for foods was performed. All formulations presented a shear-thinning behavior. Static yield stress was measured in samples with the highest fat and MWP contents, while dynamic yield stress was estimated for all formulations. Steady shear viscosity as function of shear rate was analyzed applying the Herschel–Bulkley model obtaining acceptable *RMSE* values. In addition, all formulations presented a liquid-like behavior, where loss modulus was higher than storage modulus in the range of the studied frequencies. The dependence of both moduli with the frequency was described with a power law equation, obtaining good *RMSE* values. The Cox–Merz rule was followed by control samples and formulations with the lowest fat and MWP contents (Fat 3% and MWP 3%). The other formulations deviated from the Cox–Merz rule ($|G^*(\omega)|_{\omega=\dot{\gamma}} < \tau(\dot{\gamma})$), possible due to the heterogeneity of samples. Images of each formulation and ingredients obtained by optical microscopy evidenced the presence of several phases, such as polysaccharide crystals, fat, and MWP. The average film thickness values estimated by a mechanistic mathematical model were in the range of 0.30–1.08 mm and 0.38–5.36 mm for glaze materials with fat and MWP contents, respectively. The results indicate that it may be possible to obtain alternative low-fat glaze materials for food coating processes with flow and viscoelastic properties, microstructure, and film thickness-forming capacities similar to a full-fat formulation manufactured with vegetable fat. The findings obtained in this work can be useful to control and predict the film thickness during an industrial food glazing process, reducing the amount of trial-and-error effort to obtain a desirable homogenous gloss film.

Conflicts of interest

The authors Bárbara E. Meza, Juan Manuel Peralta, and Susana E. Zorrilla declare no competing financial interest.

Acknowledgments

This research was supported partially by Universidad Nacional del Litoral (Santa Fe, Argentina), Consejo Nacional de Investigaciones Científicas y Técnicas (CONICET, Argentina), and Agencia Nacional de Promoción Científica y Tecnológica (ANPCyT, Argentina).

Nomenclature

a	rheological parameter of Eq. (3) [Pa s^b]
b	rheological parameter of Eq. (3) [-]
c	rheological parameter of Eq. (3) [Pa s^d]
d	rheological parameter of Eq. (3) [-]
g_x	gravity acceleration [m s^{-2}]
$G'(\omega)$	storage modulus [Pa]
$G''(\omega)$	loss modulus [Pa]
$\lvert G^*(\omega)\rvert$	complex modulus [Pa]
h	film thickness at the x position of the plate [m]
$\langle h \rangle$	theoretical average film thickness [m]
K	consistency index [Pa s^n]
LVR	linear viscoelastic region
MWP	microparticulated whey proteins
n	behavior index [-]
N	total number of samples
RMSE	root mean square error
S_{τ_0}	ratio of the yield stress to the maximum stress [$\tau_0/(\rho g_x h)$]
t	time [s]
x	position in the x-direction [m]
$x_{i,\text{exp}}$	i-th experimental value
$x_{i,\text{theor}}$	i-th theoretical value

Greek symbols

γ	strain [-]
$\dot{\gamma}$	shear rate [s^{-1}]
$\eta(\dot{\gamma})$	steady shear viscosity [Pa s]
$\eta'(\omega)$	loss viscosity [Pa s]
$\eta''(\omega)$	storage viscosity [Pa s]
$\lvert\eta^*(\omega)\rvert$	complex viscosity [Pa s]
ρ	density [kg m^{-3}]
τ	shear stress [Pa]
$\tau(\dot{\gamma})$	steady shear stress [Pa]
τ_0	yield stress [Pa]
$\tau_{0,d}$	dynamic yield stress [Pa]
$\tau_{0,s}$	static yield stress [Pa]
ω	angular frequency [rad s^{-1}]

References

Al-Hadithi, T.S.R., Barnes, H.A., Waiters, K., 1992. The relationship between the linear (oscillatory) and nonlinear (steady-state) flow properties of a series of polymer and colloidal systems. Colloid Polym. Sci. 270, 40–46.

Bhattacharya, S., 1999. Yield stress and time-dependent rheological properties of mango pulp. J. Food Sci. 64, 1029–1033.
Bhattacharya, S., Patel, B.K., 2007. Simulation of coating process: rheological approach in combination with artificial neural network. J. Texture Stud. 38, 555–576.
Bird, R.B., Amstrong, R.C., Hassager, O., 1987. Dynamics of polymeric fluids. In: Fluid Mechanics second ed., vol. 1 John Wiley & Sons, York, UK.
Buckman, J., Viney, C., 2002. The effect of a commercial extended egg albumen on the microstructure of icing. Food Sci. Technol. Int. 8 (2), 109–115.
CAA, 2010. Código Alimentario Argentino, Capítulo X: Alimentos Azucarados. http://www.anmat.gov.ar/alimentos/normativas_alimentos_caa.asp. Accessed 25 June 2014.
Chamberlain, E.K., Rao, M.A., 1999. Rheological properties of acid converted waxy maize starches in water and 90% DMSO/10% water. Carbohydr. Polym. 40, 251–260.
Chan, C.-M., Venkatraman, S., 2006. Coating rheology. In: Tracton, A.A. (Ed.), Coatings Technology Handbook. CRC Taylor & Francis, Boca Raton, FL.
Chin, N.L., Abdullah, R., Yusof, Y.A., 2011. Glazing effects on bread crust and crumb staling during storage. J. Texture Stud. 42, 459–467.
Cox, W.P., Merz, E.H., 1958. Correlation of dynamic and steady flow viscosities. J. Polym. Sci. 28, 619–622.
Faria, N., Pons, M.N., Feyo de Azevedo, S., Rocha, F.A., Vivier, H., 2003. Quantification of the morphology of sucrose crystals by image analysis. Powder Technol. 133, 54–67.
Ferry, J.D., 1970. Viscoelastic Properties of Polymers. John Willey & Sons, New York.
Fog-Petersen, M.S., Skibsted, L.H., 1999. Freeze- and bake-stable glazing for confectionery products characterized by differential scanning calorimetry. Eur. Food Res. Technol. 210, 114–118.
Galanakis, C.M., Tornberg, E., Gekas, V., 2010. Dietary fiber suspensions from olive mill wastewater as potential fat replacements in meatballs. LWT – Food Sci. Technol. 43, 1018–1025.
Garnier, S., Petit, S., Coquerel, G., 2002. Dehydration mechanism and crystallisation behaviour of lactose. J. Therm. Analysis Calorim. 68, 489–502.
Ghorbel, D., Barbouche, A., Riahi, H., Braham, A., Attia, H., 2011. Influence of fat content on rheological properties of molten ice cream compound coatings and thickness of solidified products. J. Food Process Eng. 34, 144–159.
Gomez, M., 2008. Low-sugar and low-fat sweet goods. In: Gülüm, S., Sahin, S.S. (Eds.), Food Engineering Aspects of Baking Sweet Goods. CRC Press, Boca Raton, FL.
Grosso, D., 2011. How to exploit the full potential of the dip-coating process to better control film formation. J. Mater. Chem. 21, 17033–17038.
IDF, 1993. Dried Milk and Dried Cream. Determination of Water Content. Standard 26A. International Dairy Federation, Brussels, Belgium.
Jahromi, S.H.R., Yazdi, F.T., Karimi, M., Mortazavi, S.A., Davoodi, M.G., Pourfarzad, A., Sourki, A.H., 2012. Application of glazing for bread quality improvement. Food Bioprocess Technol. 5 (6), 2381–2391.
Janhøj, Th, Ipsen, R., 2006. Effect of pre-heat treatment on the functionality of microparticulated whey protein I acid milk gels. Milchwissenschaft 61 (2), 131–134.
Jouppila, K., Kansikas, J., Roos, Y.H., 1997. Glass transition, water plasticization, and lactose crystallization in skim milk powder. J. Dairy Sci. 80, 3152–3160.
Karnjanolarn, R., McCarthy, K.L., 2006. Rheology of different formulations of milk chocolate and the effect on coating thickness. J. Texture Stud. 37, 668–680.
Lai, H.-M., Schmidt, S.J., 1990. Lactose crystallization in skim milk powder observed by hydrodynamic equilibria, scanning electron microscopy and ^{2}H nuclear magnetic resonance. J. Food Sci. 55 (4), 994–999.
Laneuville, S.I., Paquin, P., Turgeon, S.L., 2005. Formula optimization of a low-fat food system containing whey protein isolate-xanthan gum complexes as fat replacer. J. Food Sci. 70, S513–S519.
Lee, S.-Y., Dangaran, K.L., Krochta, J.M., 2002. Gloss stability of whey-protein/plasticizer coating formulations on chocolate surface. J. Food Sci. 67 (3), 1121–1125.
Lieske, B., Konrad, G., 1994. Microparticulation of whey protein: related factors affecting the solubility. Z. Lebensm. Forsch. 199, 289–293.
Lopes da Silva, J.A., Gonçalves, M.P., Rao, M.A., 1993. Viscoelastic behaviour of mixtures of locust bean gum and pectin dispersions. J. Food Eng. 18, 211–228.
Mathlouthi, M., Genotelle, J., 1998. Role of water in sucrose crystallization. Carbohydr. Polym. 37, 335–342.
Mead, D.W., 2011. Analytic derivation of the Cox–Merz rule using the MLD "toy" model for polydisperse linear polymers. Rheol. Acta 50, 837–866.
Meza, B.E., Peralta, J.M., Zorrilla, S.E., 2015. Rheological properties of a commercial food glaze material and their effect on the film thickness obtained by dip coating. J. Food Process Eng. 38, 510–516.
Moelants, K.R.N., Cardinaels, R., Jolie, R.P., Verrijssen, T.A.J., Van Buggenhout, S., Zumalacarregui, L.M., Van Loey, A.M., Moldenaers, P., Hendrickx, M.E., 2013. Relation between particle properties and rheological characteristics of carrot-derived suspensions. Food Bioprocess Technol. 6, 1127–1143.
Nguyen, Q.D., Boger, D.V., 1992. Measuring the flow properties of yield stress fluids. Annu. Rev. Fluid Mech. 24, 47–88.
Nickerson, T.A., Patel, K.N., 1972. Crystallization in solutions supersaturated sucrose and lactose. J. Food Sci. 37, 693–697.
Nieto, M.B., 2009. Structure and function of polysaccharide gum-based edible films and coatings. In: Embuscado, M.E., Huber, K.C. (Eds.), Edible Films and Coatings for Food Applications. Springer Science+Business Media, New York.
O'Connor, T.P., O'Brien, N.M., 2011. Fat replacers. In: W.Fuquay, J., Fox, P.F., McSweeney, P.L.H. (Eds.), Encyclopedia of Dairy Sciences, second ed. Academic Press, London, UK.
Peralta, J.M., Meza, B.E., Zorrilla, S.E., 2014a. Mathematical modeling of a dip-coating process using a generalized newtonian fluid I. model development. Ind. Eng. Chem. Res. 53 (15), 6521–6532.
Peralta, J.M., Meza, B.E., Zorrilla, S.E., 2014b. Mathematical modeling of a dip coating process using a generalized newtonian fluid II. Model validation and sensitivity analysis. Ind. Eng. Chem. Res. 53 (15), 6533–6543.
Peressini, D., Bravin, B., Lapasin, R., Rizzotti, C., Sensidoni, A., 2003. Starch-methylcellulose based edible films: rheological properties of film-forming dispersions. J. Food Eng. 59, 25–32.
Poirier, P., Giles, T.D., Bray, G.A., Hong, Y., Stern, J.F., Pi-Sunyer, X., Eckel, R.H., 2006. Obesity and cardiovascular disease: pathophysiology, evaluation, and effect of weight loss. Circulation 113, 898–918.
Raghavan, S.L., Ristic, R.I., Sheen, D.B., Sherwood, J.N.L., Trowbridge, L., York, P., 2000. Morphology of crystals of α-lactose hydrate grown from aqueous solution. J. Phys. Chem. B 104, 12256–12262.
Rao, M.A., 2007. Rheology of Fluid and Semisolid Foods: Principles and Applications. Springer Science+Business Media LLC, New York.
Renard, D., Lavenant, L., Sanchez, C., hemar, Y., Horne, D., 2002. Heat-induced flocculation of microparticulated whey proteins (MWP); consequences for mixed gels made of MWP and β-lactoglobulin. Colloids Surf. B Biointerfaces 24, 73–85.
Sanchez, C., Paquin, P., 1997. Protein and protein-polysaccharide microparticles. In: Damodaran, S., Paraf, A. (Eds.), Food Proteins and Their Applications. Marcel Dekker Inc, New York.
Sanchez, C., Pouliot, M., Gauthier, S.F., Paquin, P., 1999. Thermal aggregation of whey protein isolate containing microparticulated or hydrolysed whey proteins. J. Agric. Food Chem. 45, 2384–2392.
Sandrou, D.K., Arvanitoyannis, I.S., 2000. Low-fat/calorie foods: current state and perspectives. Crit. Rev. Food Sci. Nutr. 40 (5), 427–447.
Singer, N.S., Yamamoto, S., Latella, J., 1988. Protein product base. European Patent Applied N° 0.250.623.
Singer, N.S., 1996. Microparticulated proteins as fat mimetics. In: Roller, S., Jones, S.A. (Eds.), Handbook of Fat Replacers. CRC Press, Boca Raton, FL.
Snijkers, F., Vlassopoulos, D., 2014. Appraisal of the Cox–Merz rule for well-characterized entangled linear and branched polymers. Rheol. Acta 53, 935–946.
Spiegel, T., 1999. Whey protein aggregation under shear conditions -effects of lactose and heating temperatures on aggregate size and structure. Int. J. Food Sci. Technol. 34, 523–531.
Steffe, J.F., 1996. Rheological Methods in Food Process Engineering, second ed. Freeman Press, Miami.
Walstra, P., Wouters, J.T.M., Geurts, T.J., 2006. Dairy science and technology (Chapter 2). In: Milk Components, second ed. CRC Press, Boca Raton, FL.
Wichchukit, S., McCarthy, M.J., McCarthy, K.L., 2005. Flow behavior of milk chocolate melt and the application to coating flow. J. Food Sci. 70 (3), E165–E171.
Winter, H.H., 2009. Three views of viscoelasticity for Cox–Merz materials. Rheol. Acta 48, 241–243.
Xu, X., Liu, W., Zhang, L., 2006. Rheological behavior of Aeromonas gum in aqueous solutions. Food Hydrocoll. 20, 723–729.
Yang, X., Rogers, N.R., Berry, T.K., Foegeding, E.A., 2011. Modeling the rheological properties of Cheddar cheese with different fat contents at various temperatures. J. Texture Stud. 42, 331–348.
Yoo, B., Rao, M.A., 1995. Yield stress and relative viscosity of tomato concentrates-Effect of total solids and finisher screen size. J. Food Sci. 60 (4), 777–779.
Yu, C., Gunasekaran, S., 2001. Correlation of dynamic and steady flow viscosities of food materials. Appl. Rheol. 3, 134–140.